

Temporal variations of wall shear stress parameters in intracranial aneurysms—importance of patient-specific inflow waveforms for CFD calculations

Christof Karmonik · Christopher Yen · Orlando Diaz ·
Richard Klucznik · Robert G. Grossman ·
Goetz Benndorf

Received: 23 December 2009 / Accepted: 18 March 2010 / Published online: 14 April 2010
© Springer-Verlag 2010

Abstract

Purpose To assess reliability of wall shear stress (WSS) calculations using computational fluid dynamics (CFD) dependent on inflow in internal carotid artery aneurysms (ICA). **Materials and methods** Six unruptured ICA aneurysms were studied. 3D computational meshes were created from 3D digital subtraction angiographic images (Axiom Artis dBA, Siemens Medical Solutions). Transient CFD simulations (Fluent, ANSYS Inc.) were performed for two inflow conditions: (1) idealized averaged waveform from normal subjects (ID) and (2) patient-specific waveform (PS) measured with 2D phase contrast magnetic resonance imaging. Stability of calculation was assessed by comparing mean WSS ($\langle WSS \rangle$), temporal wall shear stress magnitude variation (ΔWSS), and oscillatory shear index (OSI, a measure of variation in the WSS direction) on the aneurysmal wall for both conditions.

Results For all cases, mean relative difference (PS–ID) of WSS ($\langle WSS \rangle$) was -15% (range -32% to 11%). Mean ΔWSS difference was -29.3% (-100% to 67%). Mean OSI difference was 7.5% (-12% to 40%). Large variations in histograms of these parameters were noted.

Conclusion For accurate calculations of WSS parameters, patient-specific information on physiological flow may be necessary. Results obtained with averaged or idealized flow waveforms may have to be interpreted with caution.

Keywords Cerebral aneurysms · Computational fluid dynamics · Magnetic resonance angiography · Digital subtraction angiography

Introduction

Computational simulations of blood flow in cerebral aneurysm is an active field of research [10, 11, 13, 17, 18, 23, 25, 30–32] motivated by the potential of assessing aneurysmal rupture risk through knowledge of hemodynamic parameters. Of those parameters, wall shear stress (WSS) magnitudes have gained particular interest: a recent study found significant larger wall areas with lower WSS in ruptured versus unruptured aneurysms of the paraclinoid and supraclinoid section of the internal carotid artery [19]. Other studies have also linked low WSS to aneurysm formation or risk of rupture [1, 20, 28]. In particular, the gradient oscillatory index [35] has recently been demonstrated to have a significant correlation with the location of aneurysm formation.

It has been suggested that WSS modulates the endothelial cell phenotype and that a WSS magnitude of less than 1.5 Pa may lead to the degeneration of the arterial wall [27].

The authors have no financial relationships to disclose.

C. Karmonik (✉) · C. Yen · R. G. Grossman
Department of Neurosurgery,
The Methodist Hospital Neurological Institute,
Houston, TX, USA
e-mail: ckarmonik@tmhs.org

C. Karmonik
Weil Medical College of Cornell University,
New York, NY, USA

O. Diaz · R. Klucznik
Department of Radiology,
The Methodist Hospital Neurological Institute,
Houston, TX, USA

G. Benndorf
Department of Radiology, Baylor College of Medicine,
Houston, TX, USA

While under normal conditions, non-pathological tissue remodeling may occur, the combination of abnormal flow patterns and genetic predisposition could lead to formation and rupture of a cerebral aneurysm [34]. To quantify WSS, computational fluid dynamics (CFD) in combination with geometrical data derived from rotational 3D digital subtraction angiographic (DSA) image data of the aneurysm and the surrounding vasculature are increasingly being used to obtain patient-specific results. The need for patient-specific geometrical data has been demonstrated by studies that reported strong variations in the inflow patterns and distribution of WSS on the aneurysmal wall dependent on the shape of the proximal segment of the parent artery [2, 10, 17, 26, 29, 36].

Besides morphology and geometry of the aneurysm and the parent artery, the volumetric flow waveform is another boundary condition for CFD simulations. Recently, it has been demonstrated that inflow variations into an aneurysm of the anterior communicating artery with two separate inflows may result in WSS changes as high as 43% [24]. The effects of WSS in aneurysm with only one inflow have not yet been systematically assessed. The majority of CFD studies on cerebral aneurysms have relied on averaged or idealized flow waveforms [2, 3, 5–8, 12, 16, 17, 28], and only selected CFD studies so far have used measured flow information [1, 20, 22, 23]. Thus, it appears important to provide an estimate for the uncertainty of WSS made by this simplification.

To explore the importance of patient-specific inflow information in CFD simulations of cerebral aneurysms with single inflow, we quantified differences of the temporal average of the WSS magnitude ($\langle WSS \rangle$), its temporal variation (ΔWSS), and the oscillatory shear index (OSI, a measure for the variation of the direction of the WSS vector over time) in CFD simulations on geometrical models of six aneurysms of the paraclinoid and supraclinoid sections of the internal carotid artery (ICA). In contrast to previous studies [24], all aneurysms investigated only had one inflow. Factors such as different strengths between inflow jets or a time difference between inflows (asymmetry in the inflow pattern) will therefore not occur, and potential differences in aneurysm hemodynamics and aneurysm wall shear stress will be due to the shape of the inflow waveform. Two inflow conditions were investigated: (1) idealized volumetric inflow waveform (ID) and (2) patient-specific inflow waveforms (PS) derived from 2D phase contrast magnetic resonance (2D pcMRI) measurements [38].

Materials and methods

Approval of the institutional review board was obtained for this study.

Patient data

Clinical images from diagnostic examinations of six unruptured saccular aneurysms at paraclinoid or supraclinoid sections of the internal carotid artery (ICA) in six patients (mean age 62 years, range 43–76, 1 male, 5 female, range of largest diameter 7.6–37.4 mm) were retrospectively collected for this study. Three of these aneurysms were terminus aneurysms (case 1, case 3, and case 6), and the remaining aneurysms were curvature aneurysms (case 2, case 4, and case 5).

2D phase contrast magnetic resonance imaging

Prior to endovascular treatment, all subjects underwent an MRI exam (1.5 T Sonata, Siemens Medical Solutions, Erlangen). From a 3D surface reconstruction based on time-of-flight localizer images (in-plane resolution 0.43×0.43 mm, slice thickness 0.5 mm), a vessel segment proximal to the aneurysm was selected for the flow measurements [39]. Dependent on the length of the cardiac cycle, 12–20 pcMRI images were acquired during the cardiac cycle (in-plane resolution 0.63×0.63 mm, slice thickness 5 mm; repetition time ranged from 41 to 82 ms). Volumetric blood flow rates were calculated by multiplying the cross-sectional vessel areas determined in each image with the blood flow velocity. The average volumetric blood flow rate was obtained as average over the cardiac cycle.

Computational fluid dynamic calculations

Diagnostic 3D DSA images (Axiom Artis dBA, Siemens Medical Solutions, Forchheim) were collected retrospectively. A 3D stereolithographic file of the aneurysm and the parent artery was constructed by single-value thresholding after image data were convoluted with a 3D Gaussian kernel to remove image artifacts and noise (Visualization Toolkit, Kitware, Inc.). Guided by mesh-independence analyses obtained with similar aneurysm models, tetrahedral meshes were created (final mesh sizes, case 1, 211,355; case 2, 156,549; case 3, 159,419; case 4, 218,810; case 5, 119,359; case 6, 282,536 volume elements). Transient Navier–Stokes equations were solved using a pressure-based, double-precision implicit solver with second-order discretization for pressure and momentum (ANSYS Fluent Inc.) [22]. Blood was modeled as an incompressible fluid with a density of $1,050 \text{ kg/m}^3$ and a viscosity of 0.004 kg/ms . Convergence of the simulations was monitored by the continuity residual and the residuals of the velocity components.

Transient simulations were performed for each case with two different waveforms: (1) an idealized waveform (ID) adapted from Ford et al. [9] as an average waveform of 17

young, normal volunteers measured with 2D pcMRI and (2) the measured patient-specific volumetric flow rate waveform from each subject (PS) interpolated by cubic splines (Matlab, Mathworks Inc.). To ensure elimination of initial transients in the CFD simulations, three cardiac cycles were simulated, and results are reported from the third cardiac cycle.

CFD data analysis

From the results of the CFD simulations, the following parameters were calculated for conditions ID and PS:

1. $\langle \text{WSS} \rangle$: the temporal mean WSS values as the average over the WSS values for one cardiac cycle.
2. ΔWSS : the standard deviation of $\langle \text{WSS} \rangle$ for one cardiac cycle.
3. OSI: the oscillatory shear index is a measure for the variation of the instantaneous WSS vector relative to the direction of the time-averaged WSS vector [14]. The OSI ranges from zero, if the instantaneous WSS vector is collinear with the average WSS vector throughout the cardiac cycle, to 0.5, if the time average of the instantaneous WSS vector is zero (no preferred direction).

Parameters 1–3 were calculated on the surface of the whole computational model. In the comparison analysis, only the aneurysm wall was considered to exclude computational inaccuracies due to inflow or outflow effects at proximal and distal artery segments. For that purpose, the aneurysm was separated from the remaining of the computational mesh by an operator-defined cut plane. At each surface point (node), first parameters 1–3 were calculated for condition ID and for condition PS, and then the difference PS–ID was calculated. Relative differences (RD) (in percent) for each parameter were calculated by

subtracting the value obtained with ID from the value obtained with PS and dividing the result by the average value from both simulation and multiplying by 100.

4. Histograms of WSS on the surface of the aneurysm: histograms of WSS have been previously used by Jou et al. to distinguish between stable and an unstable fusiform basilar aneurysms [20]. Histograms were only calculated for the aneurysm wall.

Results

Volumetric inflow waveforms

Magnitude, time of maximum flow, and length of the measured cardiac cycle varied between cases (Table 1). Average over all six cases, the duration of the cardiac cycle, minimum flow, and mean flow were in good agreement (within 1 standard deviation, except for time of maximum flow) with the corresponding values of the idealized volumetric flow waveform (Table 1).

Differences in WSS parameters between conditions ID and PS

Absolute mean and maximum values are given in Table 2 for the aneurysm wall. Minimum values were close to zero for all parameters, and cases and are not shown.

RD (Table 3) of mean $\langle \text{WSS} \rangle$ ranged from (–32%) to 11%. RD for mean ΔWSS were even larger ((–100%) to 67%); however, absolute values for this parameter were found to be relatively low compared to $\langle \text{WSS} \rangle$ (Table 2) not exceeding 0.1 Pa. Mean average RD of OSI values ranged from –12% to 40% with absolute mean difference values not exceeding 0.01 (on a scale from 0 to 1). While

Table 1 Characteristic parameters of the volumetric inflow waveforms proximal to the aneurysms measured with 2D pcMRI and of the idealized waveform

Case	Length of measured cardiac cycle [ms]	Maximum flow rate [ml/min]	Minimum flow rate [ml/min]	Mean flow rate [ml/min]
1	620	415	196	291
2	800	372	190	263
3	925	356	154	227
4	805	371	211	273
5	908	424	153	250
6	689	467	188	304
Average (1–6)	791±120	401±42	182±24	268±28
Idealized waveform	850	455	189	279

Averaged over all cases, measured parameters were in good agreement (within 1 standard deviation, except for time of maximum flow) with the corresponding parameters of the idealized waveform

Table 2 Mean and maximum values (in parenthesis) of <WSS>, ΔWSS, and OSI on the aneurysm wall obtained from simulations with the patient-specific inflow waveforms (PS) and the idealized waveform (ID)

Case	Mean <WSS> (maximum WSS) [Pa]		Mean (maximum) ΔWSS [Pa]		Mean (maximum) OSI	
	PS	ID	PS	ID	PS	ID
1	2.9 (42)	2.6 (39)	0.05 (0.8)	0.09 (1.2)	0.002 (0.24)	0.002 (0.26)
2	0.16 (13)	0.22 (16)	0.003 (0.2)	0.009 (0.6)	0.006 (0.43)	0.008 (0.42)
3	0.03 (0.7)	0.04 (1.0)	0.0007 (0.03)	0.0007 (0.02)	0.004 (0.47)	0.003 (0.45)
4	0.52 (19)	0.53 (19)	0.01 (0.3)	0.018 (0.6)	0.008 (0.46)	0.009 (0.43)
5	0.9 (10)	1.1 (12)	0.03 (0.3)	0.04 (0.4)	0.005 (0.24)	0.005 (0.20)
6	0.9 (16)	1.1 (12)	0.06 (0.9)	0.03 (0.6)	0.003 (0.40)	0.002 (0.46)

Minimum values were close to zero for all parameters and cases

mean difference values are small, pronounced differences in these parameters occurred spatially localized in regions on the aneurysm dome, (Fig. 1, center row). RD of maximum values for <WSS> averaged over the aneurysm wall ranged from (-35%) to 29% corresponding to several Pascal in absolute units. While RD of maximum values for ΔWSS and OSI were relatively large (Table 3), absolute differences were small (less than 1 Pa for ΔWSS and less than 0.06 Pa for the OSI) (for a graphical presentation, see Fig. 1, center row).

Average RD of mean <WSS> for the group of the terminal aneurysms (case 1, case 3, and case 6) and the group of the curvature aneurysms (case 2, case 4, and case 5) were very similar, -13±21% and -18±15%, respectively, as were the average RD for the mean OSI (9±27% and 6±21%). Larger variation in the results were found between the two groups for the average RD of the mean ΔWSS (3±62% versus -62±36%) and for the maxima RD of each parameter (<WSS> 0.3±32% versus -13±11%, ΔWSS 13±46% versus -65±36%, OSI -6±9% versus 8±9%).

Histograms

The shape of the histograms for WSS, ΔWSS, and the OSI on the aneurysm surface differed in all cases. The presence

of large local variations in these parameters resulted in large differences in the histograms (cases 1–6 for ΔWSS and cases 1–4 for OSI). Small differences in the 3D surface plots corresponded to histograms similar in shape (in particular WSS for cases 1–4 and 6, OSI for cases 5 and 6).

Discussion

Differences in the temporal average of the WSS magnitude exceeding 30% and similar differences in its standard deviation and in the OSI were found using patient-specific and idealized flow waveforms of the parent artery in six saccular aneurysms of the ICA. These results emphasize the need for an accurate knowledge of the volumetric inflow waveform for reliable calculations of WSS parameters. While several studies have demonstrated good agreement between in vivo measurements and CFD results [7, 22, 23], the influence of geometrical and physiological boundary conditions on the accuracy of the CFD results remains to be established. Geometrical variations of the proximal segments of the parent artery and of the aneurysm dome have been demonstrated to influence the simulated flow characteristics within the aneurysm [2, 16, 17, 29], and alternations of inflow

Table 3 Relative differences (RD) of mean and maximum (in parenthesis) of <WSS>, ΔWSS, and OSI on the surface of the aneurysm obtained from simulations with the patient-specific inflow waveforms (PS) and the idealized waveform (ID)

Case	Mean (maximum) <WSS> [%]	Mean (maximum) ΔWSS [%]	Mean (maximum) OSI [%]
1	11 (7)	-57 (-40)	0 (-8)
2	-32 (-21)	-100 (-100)	29 (2)
3	-29 (-35)	0 (40)	-12 (4)
4	-2 (0)	-57 (-67)	-12 (4)
5	-20 (-18)	-29 (-29)	0 (18)
6	-20 (29)	67 (40)	40 (-14)

Sign and absolute value of RD varied largely between parameters and cases

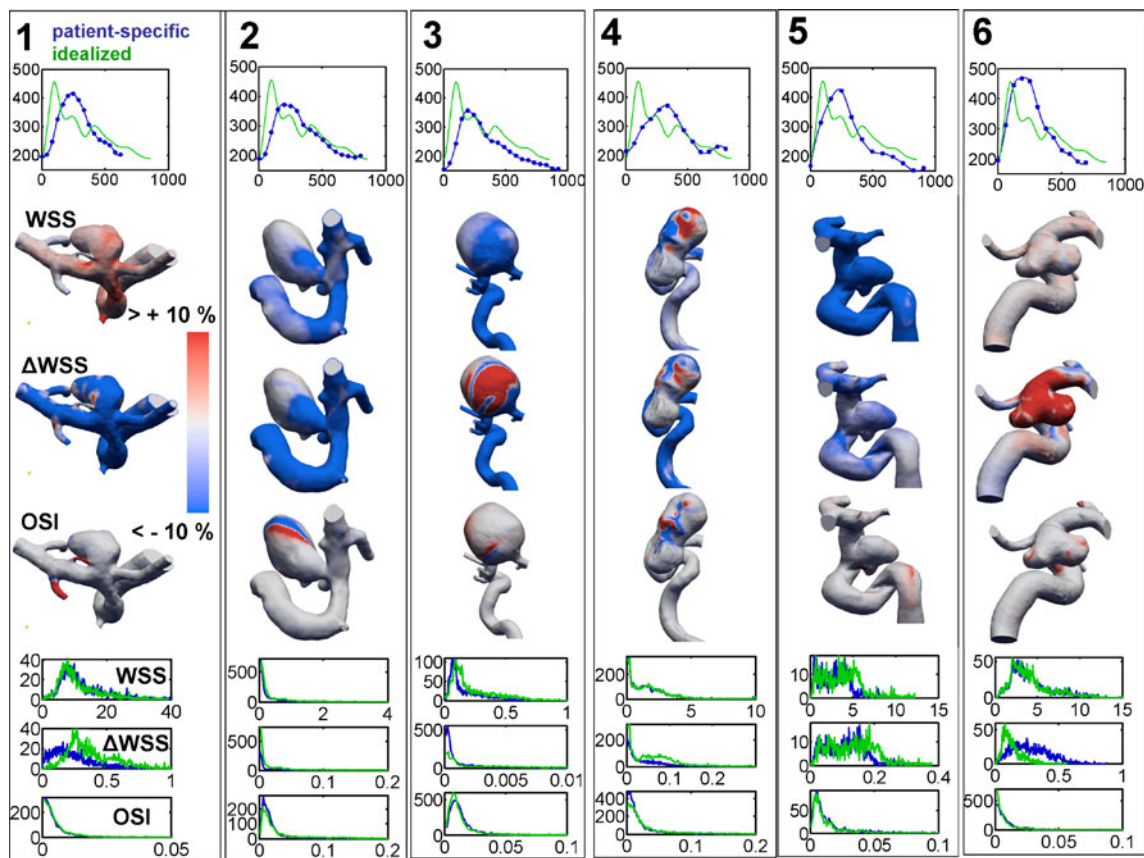


Fig. 1 Top row: Patient-specific (PS, blue) and idealized (ID, green) volumetric inflow waveforms for cases 1–6 used in the CFD simulations. Blue symbols mark times at which measurements were taken. Time (horizontal axis) is measured in milliseconds, flow rate (vertical axis) in milliliter per minute. For all cases, the measured patient-specific waveform (maximum flow, location of maximum, duration of cardiac cycle) deviated considerably from the idealized waveform. Center row: 3D surface reconstructions of the aneurysms for case 1–6 color coded by the relative differences (relative to the average of the mean values for conditions ID and PS) for $\langle WSS \rangle$, ΔWSS , and OSI (patient specific – idealized). Color scale is consistent across cases. For all cases, spatial variations can be appreciated for the results obtained with patient-specific and with idealized flow waveforms. Largest variations are visible for $\langle WSS \rangle$

and ΔWSS . In particular, for cases 1, 2, 3, and 5, relative differences exceed 10% on large sections of the computational model. Smallest differences can be observed for the OSI; however, sharply localized regions exhibit relative differences well larger than 10% (case 2 and case 4) also at the aneurysm wall. Bottom row: Histograms $\langle WSS \rangle$, ΔWSS , and OSI for the aneurysmal wall derived from the simulations using the patient-specific waveform (blue) and the idealized waveform (green). Units of the horizontal axis are Pascal for WSS and ΔWSS , OSI is a unit-less quantity. The units of the vertical axis for all three cases is “counts”. $\langle WSS \rangle$ showed smallest variations, for cases 1, 2, 4, and 6, histograms appear similar. Largest variations can be appreciated for ΔWSS resulting in entirely different histograms for cases 1 and 6

conditions have shown to modify the results for WSS magnitudes and spatial distributions [3, 21, 37].

Low WSS magnitudes and WSS histograms with predominant low WSS values have been recently correlated with aneurysmal growth [1, 20], and therefore the dependence of these parameters on the CFD boundary conditions are of particular interest. As the majority of CFD studies of cerebral aneurysmal hemodynamics has used non-patient-specific inflow waveforms [2–7, 28, 32], we focused on the differences in average WSS magnitudes, the temporal variations of the WSS, and the histograms of the WSS values on the aneurysm wall in CFD simulations using an idealized inflow waveform and using patient-specific inflow waveforms with otherwise identical boundary con-

ditions and initial parameters. The temporal variation of the WSS magnitude was characterized by the standard deviation ΔWSS computed from all values during the cardiac cycle, and the temporal variation of the direction of the WSS vector was investigated with the OSI, a measure for directional variation [14]. Large relative differences in the temporal average of WSS, corresponding to large absolute differences (several Pascal) and in ΔWSS and OSI as well as in the shape of the histograms for ΔWSS on the aneurysmal wall emphasize the need for accurate inflow boundary conditions to obtain accurate results regarding the temporal variations of the WSS. Simulations with the idealized waveform may result in spatially inaccurate distribution of WSS, which may not be able to reveal the

correct location of weak spots on the aneurysmal wall. This may be a potentially serious clinical limitation if CFD simulations should be used in clinical practice for choosing optimal endovascular devices for therapeutic treatment planning (Fig. 1).

The investigated aneurysms differed in location. Three (case 1, case 3, and case 6) were terminus aneurysms and three (case 2, case 4, and case 5) were curvature aneurysms. With the small number in each of these groups, an inter-group comparison certainly lacks statistical significance; however, from the negative mean relative deviation of Δ WSS and the negative maximum relative deviations in the \langle WSS \rangle and Δ WSS, it appears that WSS and its temporal deviation are underestimated in curvature aneurysms when using the idealized waveform. Further studies are warranted to investigate this trend in more detail.

Our models employed for the CFD simulations vary according to the location of the aneurysm and the length and number of the adjacent arteries. In particular, the length of the proximal segment varied (models 1 and 2 do not extend to the cavernous segment, while models 3–6 incorporate variable length of the cavernous segment). The variations are routed in the segmentation routine and the quality of the original 3D DSA image data.

The influence of shape and length of the proximal arterial segment on aneurysm hemodynamics has been investigated previously. A recent study by Sato et al. demonstrated that aneurysms lateral to a curve in the parent artery showed significant higher wall shear stress than aneurysms inside or outside this curve [33]. Another study by this group revealed a strong influence on the steady-state flow in cerebral aneurysms between U-shaped, twisted, or S-shaped arteries [17].

Additional work performed by Castro et al. demonstrated that a truncated parent artery (1 cm upstream from the aneurysm, parent artery replaced by a cylinder) underestimated wall shear stress and resulted in a shift of the impaction zone [2]. The authors of this study conclude that arriving at a theoretic answer to the question of an optimal entry length for complex vascular systems with current knowledge and techniques may be impossible and state that each patient-specific anatomy may have its unique solution.

Previously, we reported about a direct comparison of CFD results and 2D pcMRI flow measurements using intra-aneurysmal flow patterns [22]. Aneurysm models 1 and 2 were used in this comparison. The good agreement between measurement and simulation gives confidence that entry length effects, if at all, play a small role in these particular cases. In particular, the variations of wall shear stress, as reported here, were obtained with identical computational models when using the idealized and the patient-specific waveforms, that is, the length of the parent artery was not changed in between simulations. This fact, as well as the

validation of our simulation results with in vivo measurements, provides strong evidence that the reported wall shear stress variations are caused by differences in the inflow waveforms.

Validation and accuracy of CFD simulations remains an important topic before applying results to clinical situations. Approaches include the construction of ex vivo models where pressure and velocity measurements can be performed without the restrictions that exist in vivo. A recent study used particle-imaging velocity in models of ICA and basilar tip aneurysms constructed of clear silicone elastomer [11]. Good agreement in the simulated intra-aneurysmal flow pattern and its complex vortex dynamics with the experiment was found. 2D DSA with high frame rates (up to 15/s) is capable of visualizing intra-arterial and intra-aneurysmal contrast dynamics. Virtual angiograms, based on CFD results that mimic the flow of contrast, have recently been found to be in good agreement with flow pattern observed during intra-arterial contrast injections, in particular in respect to large intra-aneurysmal vortices and outflow effects [7]. These findings could potentially be validated by direct observations or by using intra-operative Doppler probes or novel techniques, such as laser speckle contrast analysis during a surgical intervention [15].

This study is limited by its relatively small sample size for providing representative statistical data (Tables 1, 2, and 3). A larger study including patient-specific waveforms may deviate more from or resemble closer to the here-used idealized waveform. Another potential limitation of obtaining 2D pcMRI measurements exists for ruptured aneurysms, where the need for rapid treatment precludes an additional MRI exam. However, if CFD simulation is aimed for the modeling of hemodynamics in an individual aneurysm, this study clearly demonstrates that not only patient-specific vascular *geometry*, but also patient-specific *inflow* boundary conditions, are necessary to obtain near to accurate calculations.

Conclusion

Large relative differences in the temporal variation of the WSS along the wall of saccular cerebral aneurysms can be observed when using idealized waveform and patient-specific waveforms measured with 2D pcMRI. For accurate calculations of WSS and its variations during the cardiac cycle, not only patient-specific aneurysm geometries, but also patient-specific parent artery flow data, is essential for accurate description of aneurysmal hemodynamics calculated with CFD. On the other hand, quantitative results obtained with idealized or standardized waveforms should be interpreted with great caution, in particular, when CFD simulations are used in clinical settings aiming to identify a weak spot in the aneurysmal wall, potentially prone to rupture.

References

1. Acevedo-Bolton G, Jou LD, Dispensa BP, Lawton MT, Higashida RT, Martin AJ, Young WL, Saloner D (2006) Estimating the hemodynamic impact of interventional treatments of aneurysms: numerical simulation with experimental validation: technical case report. *Neurosurgery* 59:E429–E430, author reply E429–430
2. Castro MA, Putman CM, Cebal JR (2006) Computational fluid dynamics modeling of intracranial aneurysms: effects of parent artery segmentation on intra-aneurysmal hemodynamics. *AJNR Am J Neuroradiol* 27:1703–1709
3. Castro MA, Putman CM, Cebal JR (2006) Patient-specific computational fluid dynamics modeling of anterior communicating artery aneurysms: a study of the sensitivity of intra-aneurysmal flow patterns to flow conditions in the carotid arteries. *AJNR Am J Neuroradiol* 27:2061–2068
4. Castro MA, Putman CM, Cebal JR (2006) Patient-specific computational modeling of cerebral aneurysms with multiple avenues of flow from 3D rotational angiography images. *Acad Radiol* 13:811–821
5. Cebal JR, Castro MA, Burgess JE, Pergolizzi RS, Sheridan MJ, Putman CM (2005) Characterization of cerebral aneurysms for assessing risk of rupture by using patient-specific computational hemodynamics models. *AJNR Am J Neuroradiol* 26:2550–2559
6. Cebal JR, Lohner R (2005) Efficient simulation of blood flow past complex endovascular devices using an adaptive embedding technique. *IEEE Trans Med Imaging* 24:468–476
7. Cebal JR, Pergolizzi RS Jr, Putman CM (2007) Computational fluid dynamics modeling of intracranial aneurysms: qualitative comparison with cerebral angiography. *Acad Radiol* 14:804–813
8. Dempere-Marco L, Oubel E, Castro M, Putman C, Frangi A, Cebal J (2006) CFD analysis incorporating the influence of wall motion: application to intracranial aneurysms. *Med Image Comput Assist Interv Int Conf Med Image Comput Assist Interv* 9:438–445
9. Ford MD, Alperin N, Lee SH, Holdsworth DW, Steinman DA (2005) Characterization of volumetric flow rate waveforms in the normal internal carotid and vertebral arteries. *Physiol Meas* 26:477–488
10. Ford MD, Lee SW, Lownie SP, Holdsworth DW, Steinman DA (2008) On the effect of parent-aneurysm angle on flow patterns in basilar tip aneurysms: towards a surrogate geometric marker of intra-aneurysmal hemodynamics. *J Biomech* 41:241–248
11. Ford MD, Nikolov HN, Milner JS, Lownie SP, Demont EM, Kalata W, Loth F, Holdsworth DW, Steinman DA (2008) PIV-measured versus CFD-predicted flow dynamics in anatomically realistic cerebral aneurysm models. *J Biomech Eng* 130:021015
12. Ford MD, Stuhne GR, Nikolov HN, Habets DF, Lownie SP, Holdsworth DW, Steinman DA (2005) Virtual angiography for visualization and validation of computational models of aneurysm hemodynamics. *IEEE Trans Med Imaging* 24:1586–1592
13. Funamoto K, Hayase T, Saijo Y, Yambe T (2008) Numerical experiment for ultrasonic-measurement-integrated simulation of three-dimensional unsteady blood flow. *Ann Biomed Eng*
14. He XJ, Ku DN (1996) Pulsatile flow in the human left coronary artery bifurcation: average conditions. *Journal of Biomechanical Engineering-Transactions of the Asme* 118:74–82
15. Hecht N, Woitzik J, Dreier JP, Vajkoczy P (2009) Intraoperative monitoring of cerebral blood flow by laser speckle contrast analysis. *Neurosurg Focus* 27:E11
16. Hoi Y, Woodward SH, Kim M, Taulbee DB, Meng H (2006) Validation of CFD simulations of cerebral aneurysms with implication of geometric variations. *J Biomech Eng* 128:844–851
17. Imai Y, Sato K, Ishikawa T, Yamaguchi T (2008) Inflow into saccular cerebral aneurysms at arterial bends. *Ann Biomed Eng* 36(9):1489–1495
18. Jou LD, Lee DH, Morsi H, Mawad ME (2008) Wall shear stress on ruptured and unruptured intracranial aneurysms at the internal carotid artery. *AJNR Am J Neuroradiol* 29:1761–1767
19. Jou LD, Mawad ME (2009) Growth rate and rupture rate of unruptured intracranial aneurysms: a population approach. *Biomed Eng Online* 8:11
20. Jou LD, Wong G, Dispensa B, Lawton MT, Higashida RT, Young WL, Saloner D (2005) Correlation between luminal geometry changes and hemodynamics in fusiform intracranial aneurysms. *AJNR Am J Neuroradiol* 26:2357–2363
21. Karmonik C, Benndorf G, Klucznik R, Haykal H, Strother CM (2006) Wall shear stress variations in basilar tip aneurysms investigated with computational fluid dynamics. *Conf Proc IEEE Eng Med Biol Soc* 1:3214–3217
22. Karmonik C, Klucznik R, Benndorf G (2008) Blood flow in cerebral aneurysms: comparison of phase contrast magnetic resonance and computational fluid dynamics—preliminary experience. *Rofo* 180:209–215
23. Karmonik C, Klucznik R, Benndorf G (2008) Comparison of velocity patterns in an AComA aneurysm measured with 2D phase contrast MRI and simulated with CFD. *Technol Health Care* 16:119–128
24. Karmonik C, Yen C, Grossman RG, Klucznik R, Benndorf G (2009) Intra-aneurysmal flow patterns and wall shear stresses calculated with computational flow dynamics in an anterior communicating artery aneurysm depend on knowledge of patient-specific inflow rates. *Acta Neurochir (Wien)* 151(5):479–485
25. Kim M, Taulbee DB, Tremmel M, Meng H (2008) Comparison of two stents in modifying cerebral aneurysm hemodynamics. *Ann Biomed Eng* 36:726–741
26. Liou TM, Li YC, Juan WC (2007) Numerical and experimental studies on pulsatile flow in aneurysms arising laterally from a curved parent vessel at various angles. *J Biomech* 40:1268–1275
27. Malek AM, Izumo S (1995) Control of endothelial cell gene expression by flow. *J Biomech* 28:1515–1528
28. Mantha A, Karmonik C, Benndorf G, Strother C, Metcalfe R (2006) Hemodynamics in a cerebral artery before and after the formation of an aneurysm. *AJNR Am J Neuroradiol* 27:1113–1118
29. Meng H, Wang Z, Kim M, Ecker RD, Hopkins LN (2006) Saccular aneurysms on straight and curved vessels are subject to different hemodynamics: implications of intravascular stenting. *AJNR Am J Neuroradiol* 27:1861–1865
30. Mitsos AP, Kakalis NM, Ventikos YP, Byrne JV (2008) Haemodynamic simulation of aneurysm coiling in an anatomically accurate computational fluid dynamics model: technical note. *Neuroradiology* 50:341–347
31. Ortega J, Hartman J, Rodriguez J, Maitland D (2008) Post-treatment hemodynamics of a basilar aneurysm and bifurcation. *Ann Biomed Eng* 36(9):1531–1546
32. Radaelli AG, Augsburger L, Cebal JR, Ohta M, Rufenacht DA, Balossino R, Benndorf G, Hose DR, Marzo A, Metcalfe R, Mortier P, Mut F, Reymond P, Socci L, Verheghe B, Frangi AF (2008) Reproducibility of haemodynamical simulations in a subject-specific stented aneurysm model—a report on the Virtual Intracranial Stenting Challenge 2007. *J Biomech* 41:2069–2081
33. Sato K, Imai Y, Ishikawa T, Matsuki N, Yamaguchi T (2008) The importance of parent artery geometry in intra-aneurysmal hemodynamics. *Med Eng Phys* 30:774–782
34. Sforza DM, Putman CM, Cebal JR (2009) Hemodynamics of cerebral aneurysms. *Annu Rev Fluid Mech* 41:91–107
35. Shimogonya Y, Ishikawa T, Imai Y, Matsuki N, Yamaguchi T (2009) Can temporal fluctuation in spatial wall shear stress gradient initiate a cerebral aneurysm? A proposed novel hemody-

- dynamic index, the gradient oscillatory number (GON). *J Biomech* 42:550–554
36. Valencia A, Morales H, Rivera R, Bravo E, Galvez M (2007) Blood flow dynamics in patient-specific cerebral aneurysm models: the relationship between wall shear stress and aneurysm area index. *Med Eng Phys* 30(3):329–340
 37. Venugopal P, Valentino D, Schmitt H, Villablanca JP, Vinuela F, Duckwiler G (2007) Sensitivity of patient-specific numerical simulation of cerebral aneurysm hemodynamics to inflow boundary conditions. *J Neurosurg* 106:1051–1060
 38. Zhao M, Amin-Hanjani S, Ruland S, Curcio AP, Ostergren L, Charbel FT (2007) Regional cerebral blood flow using quantitative MR angiography. *AJNR Am J Neuroradiol* 28:1470–1473
 39. Zhao M, Charbel FT, Alperin N, Loth F, Clark ME (2000) Improved phase-contrast flow quantification by three-dimensional vessel localization. *Magn Reson Imaging* 18:697–706

Comment

How to identify intracranial aneurysms at risk of rupture from those that never will rupture, remains a significant clinical challenge that has very drastic implications for the life of patients with aneurysms. Recent studies of the pathobiology of the aneurysm wall, as well as

the emerging field of computational hemodynamic models, have tried to develop a reliable solution for the prediction of rupture-risk.

As with all simulations and mathematical models, the main question regarding their usefulness for clinical applications is how accurately they represent the reality. In the field of computational fluid dynamics, it has been well known that the models are as accurate as their input parameters – e.g. the geometry of the vasculature and of the aneurysm, the flow conditions, and the other boundary conditions. Because accurate, non-invasive measurements for some of these parameters are difficult – especially for the inflow velocities and vectors – there is a strong urge to simplify the computational models by making generalizations and assumptions for those parameters that are too difficult to actually measure.

The study by Karmonik et al. elegantly demonstrates how important it is to have accurate, patient specific boundary conditions for the computational fluid dynamic models. Otherwise you will end up with a very elegant appearing model that has little to do with the real distribution and intensity of mechanical stress in the aneurysm, and hence might easily mislead in the clinical decision making of which aneurysm to operate, when, and what site of the aneurysm should be especially well occluded.

Juhana Frösen
Mika Niemelä
Juha Hernesniemi
Helsinki, Finland